A Low-Complexity Approach for Color Display of Hyperspectral Remote-Sensing Images Using One-Bit Transform Based Band Selection

Begüm Demir, *Student Member, IEEE*, Anıl Çelebi, *Student Member, IEEE* and Sarp Ertürk, *Member, IEEE*

Abstract—This paper presents a new approach for color display of hyperspectral images. It is proposed to use the one-bit transform of hyperspectral image bands to select three suitable bands for RGB display. The proposed approach has low complexity and is very suitable for hardware implementation. A dedicated hardware architecture that computes the transitions in the one-bit transform of hyperspectral image bands to determine bands that contain more information and the corresponding FPGA implementation of the proposed architecture is presented. In the proposed approach, less-structured bands are initially eliminated using the total number of transitions in the one-bit transform of hyperspectral image bands. Then, three suitable bands are selected from within this remaining set of well structured bands, for RGB color display. The proposed approach provides a new method to facilitate color display of hyperspectral images, that has very low-complexity.

***Index Terms*—Display of hyperspectral images, one-bit transform, low-complexity.**

I. Introduction

Hyperspectral imaging sensors acquire data corresponding to hundreds of continuous narrow spectral bands [1]. Therefore, it is not possible to directly display hyperspectral images with conventional displays that typically display color images using three bands; namely red, green and blue (RGB).

There are basically two methods available for the color display of hyperspectral images. The first approach is to perform some segmentation or classification on the hyperspectral image and display each segment/class with a different color. However, efficient segmentation/classification of the large amount of data captured in hyperspectral images is usually time consuming and complex. Furthermore, the natural appearance of the scene is usually lost if only a different color is used to represent each segment/class for display. The second approach is to obtain three representative bands and use these bands as RGB components for color display. These three bands can directly be three individual bands from the hyperspectral image, or they can be combinations of original bands. This approach is likely to result in loss of information as it can be regarded as the mapping of hyperspectral images with N components into images with only three components, so that the mapping is many-to-one. In this case it is important to obtain three appropriate bands that preserve information and enable interpretability [2], preferably with a low-complexity method.

Principal Components Analysis (PCA) has commonly been used to obtain three new bands, that are actually the linear combination of original hyperspectral bands constructed using the Principal Component Transform (PCT), for hyperspectral image visualization [3-6]. In [3], it is noted that the PCT performance drops for poorly correlated data, and the correlation between hyperspectral bands is exploited by initially partitioning the entire data into subgroups of highly correlated bands and PCT is conducted separately on each subgroup. Important features are then selected from each transformed subgroup making use of variance information or separability; and these features are regrouped, after which the entire process is repeated until finally the most informative three features are used for color composite display. The principal component based display strategy for spectral imagery proposed in [4] maps the first three principal components to the HSV or RGB color spaces. Fusion of hyperspectral data by means of partitioning the hyperspectral bands into three subgroups prior to principal components transformation (PCT), and using the first principal component of each subgroup for RGB hyperspectral image visualization is presented in [5]. Three different portioning methods: equal subgroups, maximum energy partitioning and partitioning based on spectral signature, have been employed for this purpose. In [6] it is proposed to whiten the noise before PCA, which is equivalent to rank the principal components in terms of signal-to-noise ratio, for hyperspectral image visualization.

PCA has very high computational complexity because it requires finding the eigenvectors and eigenvalues of the covariance matrix. Therefore it is usually impossible to use a PCA based approach for large data sets without initially partitioning the data set.

In [7], Independent Component Analysis (ICA), correlation coefficient and mutual information have been used to fuse the information from a large number of bands to three bands for the visualization of hyperspectral images. The design goals for hyperspectral image display systems and a display method using fixed linear spectral weighting envelopes is reported in [8]. A visualization technique that utilizes double color layers to integrate the mixture information (i.e., end members and their abundances) for each pixel for display has been studied

This work was supported by the Scientific and Technological Research Council of Turkey (TUBITAK) under the "Hyperspectral Classification, Segmentation and Recognition" project with contract no. EEEAG/107E011.

in [9]. In [10], methods to display hyperspectral images by linear projection onto basis functions are explored. Instead of PCA which provides a data adaptive projection, projections with fixed basis functions based on optimizing criteria in the perceptual color space and the standardized device color space are presented.

It is proposed in this paper to utilize a one-bit transform (1BT) based approach for low-complexity selection of suitable bands for the RGB color display of hyperspectral images. Initially, relatively well-structured bands are obtained using the 1BT of each band. A dedicated hardware implementation for this approach is also presented. Finally, three suitable bands are selected from within this set of well-structured bands for RGB display of the hyperspectral image. The proposed 1BT based approach provides a very low-complexity method for effective color display of hyperspectral images, that is particularly suitable for dedicated hardware implementation.

II. The Proposed Approach

In the proposed approach it is aimed to obtain three appropriate bands from all hyperspectral image bands that will preserve information and enable interpretability. A low-complexity approach is targeted by making use of single bit-depth representations of hyperspectral image bands obtained using the one-bit transform (1BT). Using the 1BT it is aimed to make use of the property that the human visual system (HVS) perceives variations as interesting only up to a certain point and then ignores these as noise. Shannon's entropy measures have been extended to second-order measures because of this feature; and the second order entropy that penalizes excessive variations has been used to more effectively identify information in images [11]. In this paper it is proposed to make use of the 1BT to identify hyperspectral image bands that do not contain comparatively excessive spatial variations and are therefore regarded to be well-structured.

A. Obtaining Well-Structured Image Bands using 1BT

1BT based representations of image frames have mainly been used so far for block motion estimation in video coding to provide a reduction in computational complexity [12-15]. The first 1BT transform based approach proposed in [12], used the block mean as threshold value in image frames to represent pixels with a single bit-plane. In [13] a more effective 1BT has been proposed, where the original image frames have been compared with their multi band-pass filtered versions to construct one-bit/pixel representations. A 17×17 sized multi band-pass filter kernel which is used to filter the image frames is defined in the form of

$$K(i,j)=\begin{cases}1/25, \text{ if } i,j \in [0,4,8,12,16] \\ 0, \text{ otherwise}\end{cases} \quad (1)$$

The frequency response of this filter is shown in Fig. 1, where the multiple pass-bands are clearly visible. This multi band-pass structure also facilitates invariance to the spatial resolution (size) of the image.

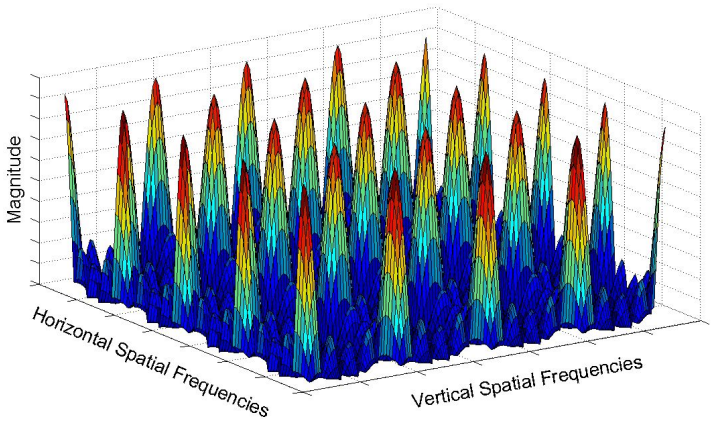

Fig.1. The magnitude frequency response of the 1BT filter.

One-bit representations of image frames are then obtained as

$$B(i,j)=\begin{cases}1, \text{ if } I(i,j)\geq I_F(i,j) \\ 0, \text{ otherwise}\end{cases} \quad (2)$$

where $I_F(i,j)$ is the filtered form of the image frame $I(i,j)$ and (i,j) are used as spatial indices. This idea is further improved for motion estimation by the multiplication free 1BT proposed in [14] and constrained 1BT proposed in [15].

1BT approaches have been successfully utilized for motion estimation in video because they capture the overall structural information of the image quite well. In this paper it is proposed to make use of 1BT representations to obtain well-structured hyperspectral image bands suitable for the color display of available information. For this purpose, the 1BT representation of each hyperspectral image band is obtained by applying the 17×17 sized multi band-pass filter kernel given in (1) to each hyperspectral band and comparing the result against the original image band, in order to obtain one-bit representations of hyperspectral image bands using (2).

Fig. 2 and Fig. 3 show example 1BT results for sample bands of the AVIRIS data set collected over Cuprite, NV, and the Indian Pine hyperspectral data set (a hyperspectral image which is taken over northwest Indiana's Indian Pine test site), respectively. For both hyperspectral images, 1BTs of one less-structured and one well-structured image band are shown. It is clearly seen that 1BTs of less-structured bands have a rather noisy appearance.

As a measure of band characteristics, the spatial bit transitions in 1BTs (changes from 1 to 0, and vice-versa) are counted and the total number of transitions in horizontal and vertical directions of each band is used as a measure of structure. If the total number of transitions in the 1BT of an image band

with band index l is shown as $A(l)$, it can be formulated as in (3).

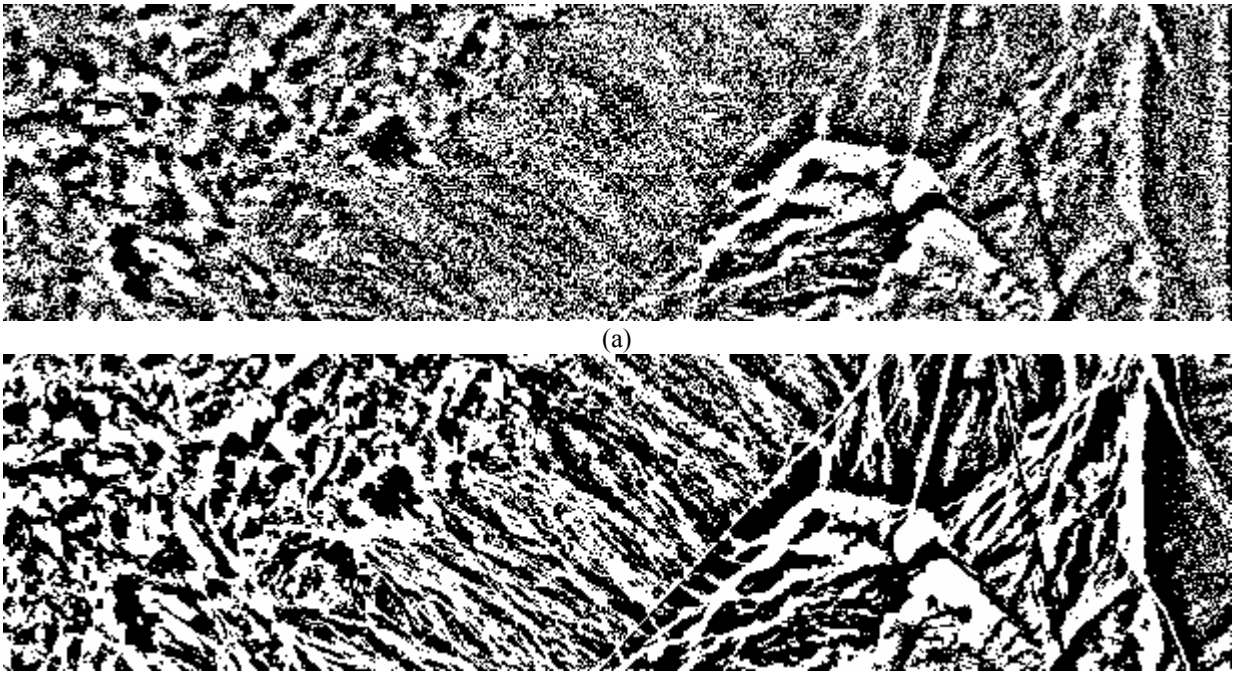

(a)

(b)

Fig.2. Example 1BTs of (a) Less-structured band (band #107) (total transition number is 67436) (b) Well-structured band (band #106) (total transition number is 39925) for the Cuprite data.

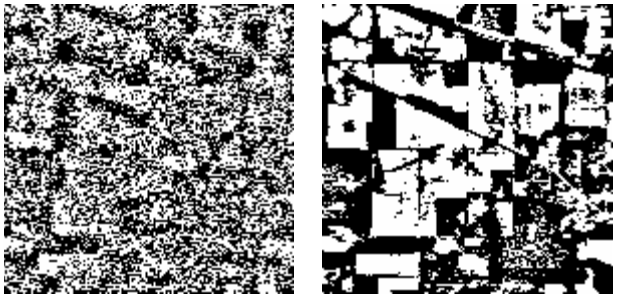

(a) (b)

Fig.3. Example 1BTs of (a) Less-structured band (band #109) (total transition number is 16465) (b) Well-structured band (band # 167) (total transition number is 6698) for the Indian Pine data.

$$A(l) = \sum_i \sum_j B_l(i,j) \oplus B_l(i-1,j) + \sum_i \sum_j B_l(i,j) \oplus B_l(i,j-1) \quad (3)$$

Here, B_l shows the 1BT of image band l, $\oplus$ represents the Boolean exclusive-or (EX-OR) operation, and (i,j) are used as spatial indices with the summation taking place over the entire image dimensions. Because of the Boolean nature, this process has very low-complexity and is particularly suited for dedicated hardware implementation.

The total number of transitions is then compared against a local threshold to decide which bands to keep and which bands to discard. Therefore, after the total number of transitions in the 1BTs of all hyperspectral bands are obtained for a certain data set, the local thresholds can be computed as a moving-average. The utilization of a moving average as local threshold is a quite common local thresholding approach [16]. The local threshold utilized in this paper can be expressed in the form of

$$t(l) = \frac{1}{7} \sum_{n=-3}^{3} A(l+n) \quad (4)$$

which is basically a moving average of size 7. Because there is typically high correlation between neighbor spectral bands in hyperspectral images, the local thresholding approach ensures that more informative bands in local neighborhoods are selected, thereby discarding, sometimes similar, less informative bands. Image bands are regarded to be well-structured and retained if their $A(l)$ values are below a threshold $T(l)$ in the form of

$$S(l) = \begin{cases} 1, \text{ if } A(l) < T(l) \\ 0, \quad \text{otherwise} \end{cases} \quad (5)$$

where $T(l)$ shows the threshold values and $S(l)$ indicates if the image band l is well-structured. Note that, the threshold values are set as $T(l) = a \times t(l)$ where a is a constant used as threshold weighting factor to allow flexibility in the number

of retained bands. Because the purpose of this step of the approach is to obtain an initial (rough) set of relatively well-structured bands, there are no strict limits on the values of the moving average window size and a parameters.

The thresholds which are obtained in this form, as weighted local averages, are shown in Fig. 4 and Fig. 5 with the corresponding total number of transitions for the Indian Pine and Cuprite data sets, respectively. Hyperspectral image bands that have a transition number above the threshold are assigned to be less-structured and are discarded, while bands that have a total transition number below the threshold are retained (regarded as well-structured) and forwarded to the next step.

Note that a larger weighting factor, a, will allow more bands to be kept as well-structured at the cost of a larger computational load in the next step, while a lower weighting factor will discard more bands reducing the computational load in the following step possibly at a cost of facilitating the display of slightly less information. The moving average window size and a parameters are set empirically in this paper, and it is observed that the same a parameters can be used for both test hyperspectral data sets, resulting in a different number of bands being forwarded to the next step. Alternatively, it is also possible to change the a value for different hyperspectral images to have always the same number of bands being forwarded to the next step.

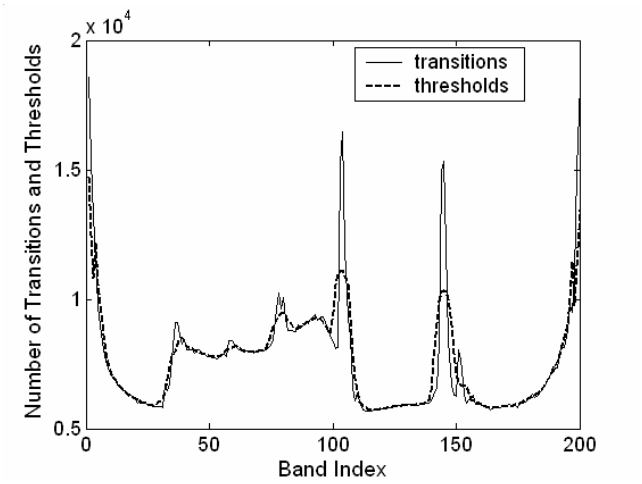

Fig. 4. Total number of transitions and transition thresholds for 1BTs obtained for the Indian Pine data.

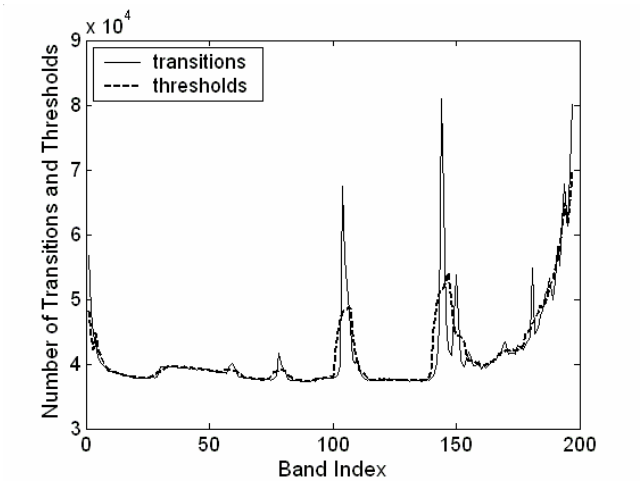

Fig. 5. Total number of transitions and transition thresholds for 1BTs obtained for the Cuprite data.

B. Selecting three suitable bands for Color Display

In the second step, three suitable bands are selected for the RGB display of the hyperspectral image from within the well-structured image band set forwarded from the previous step. Although all image bands forwarded to this step are relatively well-structured, the aim is to select three bands so that as much information as possible can be displayed if these bands are used as the red, green and blue bands of the RGB color image. For this purpose, the three image bands that are the least alike from the well-structured bands are selected in this step.

To obtain the least alike three bands of the well-structured data set, a correlation measure is used. For low-complexity, the correlation is computed over the 1BTs of the well-structured hyperspectral image bands. Because the 1BTs of image bands provide binary representations, the correlation computation turns into a simple sum of bitwise EX-OR computations between the 1BTs of image pixels located at the same spatial location of different image bands.

In this step, initially the two least similar bands are selected. For this purpose the sum of the EX-OR result between all possible well-structured image bands is computed. The two bands that give that highest total EX-OR result will have the largest difference and are selected as the two least similar well-structured image bands. These bands constitute two of the bands to be used in the color display phase. The third band is selected from the remaining well-structured bands as the band which is again least alike to the already selected two bands. For this purpose the total sum of the EX-OR results of the remaining bands with the first and second selected bands are added up, and the band giving the largest sum is selected as the third band to be used for color display. Note that, in case two different bands have the same total sum of EX-OR results with the first and second bands, it is furthermore possible to consider their distances to the first and second band individually. In this case it is possible to additionally consider the ratio of the distances to the first band and second band, and select the band that has a ratio closer to unity. This will ensure that in case of equality, a mid-point band is

selected rather than a band close to the first (or second) band. An alternative is to use the minimum of the sum of the inverse of EX-OR results, which has been observed to give the same bands in the experimental results.

III. HARDWARE ARCHITECTURE

The proposed algorithm used for obtaining well-structured hyperspectral image bands is particularly suitable for hardware implementation because of its binary and regular nature. The proposed hardware architecture that computes the transitions in the one-bit transforms of the hyperspectral image bands according to (3) is shown in Fig. 6.

The implementation of (3) includes multiple sequential summations of the EX-OR results of consecutive (horizontal or vertical) image pixels of the 1BTs. If 1BTs have a size of $M \times N$ pixels, a total of $2(M \times N)+1$ sequential summations are required. It is seen in Fig. 6 that the horizontal and vertical transitions are counted on separate parts of the hardware, in parallel. Therefore the left hand side of the architecture shown in Fig. 6 has a data path size determined by the first dimension of the image (*M*), while the right hand side has a data path determined by the second dimension of the image (*N*). The total processing delay incurred by the hardware is therefore directly determined by the larger image dimension (horizontal or vertical). Results in this paper will be given for a hardware architecture that is implemented for an image size of 145×145 pixels, taking the Indian Pine hyperspectral data set into account. In this case, 145 sequential summations for the hardware implementation are necessary to obtain the $A(l)$ value of an image band. In Fig. 6 it is shown that the Boolean EX-OR operations are performed by the EX-OR array, all in parallel, as this is the first step of the calculation of the total vertical/horizontal transitions.

Parallel counter architectures are suitable to accomplish the desired summation operation with a high performance. A $(p \mid q)$ parallel counter is a combinatorial logical module that determines how many of its p inputs are in the logical *one* state, expressing the result as a binary parallel number at its q outputs [17]. A parallel counter can be viewed as a multiple-word input adder with 1-bit words [18].

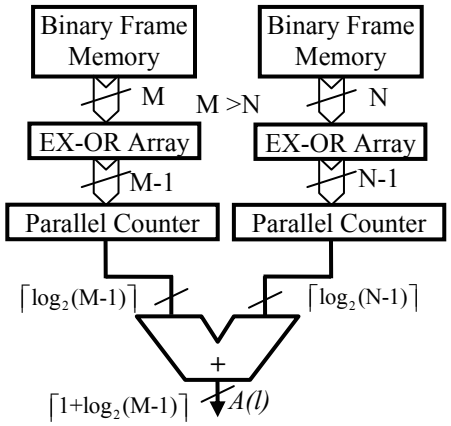

Fig. 6. Proposed architecture for calculation of $A(l)$ values of individual bands, where $\lceil x \rceil$ denotes the smallest integer i such that $i \geq x$.

In [19] a parallel counter architecture referred to as *carry shower* is implemented with full and half adders. The method used in [19] is shown for a $(31 \mid 5)$ parallel counter in Fig. 7. This approach groups counter inputs into $\lfloor p/3 \rfloor$ sets of three lines each, which are input to full adders (where $\lfloor x \rfloor$ denotes the largest integer less then or equal to x). The $\lfloor p/3 \rfloor$ sum and $\lfloor p/3 \rfloor$ carry outputs of the full adders and any other unprocessed inputs to the counter are grouped into threes and applied to the second (smaller) set of full adders, etc. The number of full adders to realize a $(p \mid q)$ parallel counter is derived in [19] to be less then or equal to p.

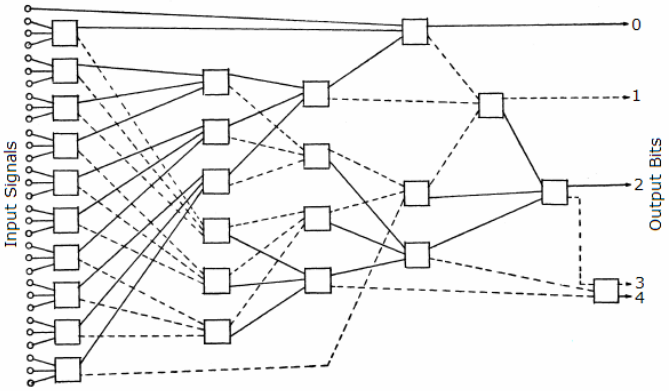

Fig. 7. Carry shower circuit for $p = 31$.

In [20], large parallel counters with up to 1022 inputs are designed based on different base counter types, e.g. $(3 \mid 2)$, $(7 \mid 3)$, $(31 \mid 5)$. It has been concluded that parallel counters designed based on the smallest counter cells, i.e. $(3 \mid 2)$ and $(2 \mid 2)$, have the best $area \times delay$ performance. The total delay of the parallel counter is equal to the sum of individual block delays of all levels of the parallel counter architecture.

The delays of synthesized blocks are obtained as

approximately $0,411ns$ and $1,635ns$ for the $(3|2)$ counter and the final adder, respectively. The delays of the $(3|2)$ counter and the $(2|2)$ counter are the same because of the technology of the FPGA on which the blocks are implemented. The total delay of the parallel counter is obtained as

$$D_{tot} = D_{add} + (L-1) \times D_{bc} + D_{2c} \quad (6)$$

where D_{tot}, D_{add}, D_{bc}, and D_{2c} show the total delay, and the delays of the final adder, base counter and $(2|2)$ counter, respectively. Here, L denotes the number of levels of the parallel counter. For an image size of 145×145 pixels, 144 EX-OR results are obtained for each row or column of the image, that need to be summed. Because in this case the maximum sum can be represented with 8 bits, a $(144|8)$ sized parallel counter is required. Because there are 11 levels in the hierarchy of the parallel counter of size $(144|8)$, the total delay of the system is obtained to be approximately $6,156ns$. The combinational path delay of the parallel counter dominates the maximum clock frequency of the hardware. Thus the maximum clock frequency of the hardware in this case is approximately 162 MHz. For an $M \times N$ pixel sized image with $M \geq N$, the proposed hardware architecture needs only M cycles to perform the $2(M \times N)+1$ operations of (3).

IV. Experimental results

The effectiveness of the proposed approach is evaluated using two different hyperspectral data sets. The first data set is taken over northwest Indiana's Indian Pine test site in June 1992 [21]. This data consists of 145×145 pixels with 220 bands. The number of bands is initially reduced to 200 bands by removing bands covering water absorption and noisy bands. The second data set is the last part of the AVIRIS data set collected over Cuprite, NV. This data contains 614×158 pixels with 224 spectral bands. After removing bands affected by atmosphere, 197 bands are retained for this set.

After the first step of the proposed approach, which determines well-structured hyperspectral image bands, 25 bands are retained for the Indian Pine data and 15 bands are retained for the Cuprite data. For both sets, the same a constant is used as threshold weighting factor, which is set to 0.95 to provide a reasonable balance between complexity and selectivity. In the next step, the three bands to be used for RGB display are selected from these well-structured bands. Table I shows the band index values for image bands retained after the first and second band selection steps for the Indian Pine and Cuprite data sets.

Although it is possible to assign the three obtained bands randomly to the red, green and blue components of the image, a standard approach is preferable, particularly for comparative evaluation. Therefore we preferred to make this assignment according to the standard deviation of each band. The band with the highest standard deviation is assigned to the red component, the band with the second highest standard deviation is assigned as the green component, and the band with the lowest standard deviation is assigned as the blue component. This assignment procedure is utilized for the proposed approach as well as the PCA based display method used for comparison, to provide consistency.

Fig. 8 shows the three selected bands, their 1BTs and the RGB color image of these bands for the Indian Pine data set. The bands with indices 5, 75 and 169 shown in Fig. 8 (a), Fig. 8 (b), and Fig. 8 (c) are used as red, green and blue components for the Indian Pine data. Fig. 9 shows the three selected bands and the RGB color image of these bands for the Cuprite data set. The bands with indices 216, 152, 116 shown in Fig. 9 (a), Fig. 9 (b), and Fig. 9 (c) are used as red, green and blue components for the Cuprite data.

PCA based image visualization of the hyperspectral images obtained by mapping the first three principal components to the RGB color space is also performed for comparison. Visualization results for the proposed approach and the PCA based approach are shown together in Fig. 10. Because PCA could not be applied to the entire Cuprite data due to high complexity resulting from the large horizontal and vertical data dimension, a sub-image was used for comparative evaluation. It is seen that the proposed approach displays about equally as much detail as observed with the PCA based approach, but has a much lower computational complexity. While the proposed approach revealed black regions for this data set, for practical purposes a black colored region has no different meaning from a red colored region because a simple mapping to RGB components is carried out.

It is reported in [7] that the correlation between RGB components can be used as a measure of success for methods that are proposed for color display of hyperspectral images, because natural color images have typically high correlation between RGB components. Table II and Table III show the correlation coefficients between the RGB components of the Indian Pine image for the proposed and PCA based approaches. Table IV and Table V show the correlation coefficients between the RGB components of the sub-image cut out from the Cuprite data, for the proposed and PCA based approaches. It is seen that the proposed approach provides much higher correlation values compared to the PCA based approach. Table VI shows the correlation coefficients between the RGB components of the entire Cuprite image obtained with the proposed approach (which can not be accomplished with the PCA based approach because of computational complexity), and it is seen that in this case again high correlation is obtained.

V. Conclusion

This paper proposes a new approach for the color display of hyperspectral images with low complexity. The approach is based on using the one-bit transforms of hyperspectral image

bands to select three suitable bands for RGB display. Because the selection of image bands is performed entirely over 1BT representations using mostly Boolean operations, the computational complexity is very low and the proposed approach is furthermore very suitable for dedicated hardware implementation.

ACKNOWLEDGMENT

The authors would like to thank D. Landgrebe for providing the AVIRIS Indian Pine data [21].

REFERENCES

[1] D. A. Landgrebe, *Signal Theory Methods in Multispectral Remote Sensing*, John Wiley & Sons, Hoboken, NJ, USA, 2003.

[2] N.P. Jacobson, and M.R. Gupta, "SNR-Adaptive linear fusion of hyperspectral images for color display," *IEEE International Conference on Image Processing*, San Antonio, TX, vol. III, pp. 477- 480, 2007.

[3] X. Jia and J. A. Richard, "Segmented principal components transformation for efficient hyperspectral remote-sensing image display and classification," *IEEE Trans. Geoscience and Remote Sensing*, vol. 37, no. 1, pp. 538-542, Jan. 1999.

[4] J. S. Tyo, A. Konsolakis, D. I. Diersen, and R. C. Olsen, "Principal components-based display strategy for spectral imagery," *IEEE Trans. Geoscience and Remote Sensing*, vol. 41, no. 3, pp. 708–718, Mar. 2003.

[5] V. Tsagaris, V. Anastassopoulos, and G. A. Lampropoulos, "Fusion of hyperspectral data using segmented PCT for color representation and classification," *IEEE Trans. Geoscience and Remote Sensing*, vol.43, no.10, pp. 2365-2375, Jan. 2005.

[6] S. Cai, Q. Du, R. Moorhead, M. J. Mohammadi-Aragh, and D. Irby, "Noise-adjusted principal component analysis for hyperspectral remotely sensed imagery visualization," in *Proc. IEEE Vis. Conf. (Compendium)*, 2005, pp. 119–120.

[7] Y. Zhu, P. K. Varshney, and Hao Chen, "Evaluation of ICA based fusion of hyperspectral images for color display," in *10th International Conference on Information Fusion*, Quebec, Canada, pp. 1-7, 2007.

[8] N. P. Jacobson and M. R. Gupta, "Design goals and solutions for display of hyperspectral images," *IEEE Trans. Geoscience and Remote Sensing*, vol. 43, no. 11, pp. 2684-2692, Nov. 2005.

[9] S. Cai, Q. Du, and R.J.Moorhead, "Hyperspectral imagery visualization using double layers", *IEEE Trans. Geoscience and Remote Sensing*, vol. 45, no. 10, pp. 3028–3036, Oct. 2007.

[10] N. P. Jacobson, M. R. Gupta, and J. B. Cole, "Linear fusion of image sets for display," *IEEE Trans. Geoscience and Remote Sensing*, vol. 45, no. 10, pp. 3277-3288, Nov. 2007.

[11] A. Mishra and S. Rakshit, "Fusion of noisy multi-sensor imagery," *Defence Science Journal,* vol. 58, no. 1, pp. 136-146, Jan. 2008.

[12] J. Feng, K.-T. Lo, H. Mehrpour, and A. E. Karbowiak, "Adaptive block matching motion estimation algorithm using bit plane matching," *in Proc. ICIP*', Washington, DC, USA, vol. 3, pp. 496–499, 1995.

[13] B. Natarajan, V. Bhaskaran, and K. Konstantinides, "Low-complexity block-based motion estimation via one-bit transforms," *IEEE Trans. Circuits Syst. Video Technol*., vol. 7, no. 4, pp. 702–706, Aug. 1997.

[14] S. Ertürk, "Multiplication-free one-bit transform for low-complexity block-based motion estimation," *IEEE Signal Processing Letters*, vol. 14, no. 2, pp.109-112, Feb. 2007.

[15] O. Urhan and S. Ertürk, "Constrained one-bit transform for low-complexity block motion estimation," *IEEE Trans. Circuits and Systems for Video Technology*, vol. 17, no. 4, pp.478-482, Apr. 2007.

[16] R.C. Gonzalez, R.E. Woods, and S.L. Eddins, *Digital Image Processing Using Matlab*. Pearson Prentice Hall, 2004.

[17] L. Dadda, "Some schemes for parallel multipliers," *Alta Frequenza*, vol. 34, pp. 349-356, Mar. 1965.

[18] E. E. Swartzlander, Jr., "Parallel counters," *IEEE Trans. Computers*, vol. C-22, pp. 749-751, Nov. 1973.

[19] C. C. Foster, and F. D. Stockton, "Counting responders in an associative memory," *Transactions on Computers*, vol. C-20, pp. 1580-1583, Dec. 1971.

[20] R. F. Jones, Jr. and E. E. Swartzlander, Jr., "Parallel counter implementation," *Journal of VLSI Signal Processing*, vol. 7, pp. 223-232, Oct. 1994.

[21] AVIRIS NW Indiana's Indian Pines 1992 data set [Online]. Available:ftp://ftp.ecn.purdue.edu/biehl/MultiSpec/92AV3C (original files) and ftp://ftp.ecn.purdue.edu/biehl/PC_MultiSpec/ThyFiles.zip (ground truth).

Begüm Demir (S'06) received her B.S. and M.Sc. degrees in Electronic and Telecommunication Engineering from Kocaeli University, in 2005 and 2007 respectively. She is still a Ph.D. student in Electronic and Telecommunication Engineering at Kocaeli University. In July, 2005 she has joined KULIS (Kocaeli University Laboratory of Image and Signal processing) as a researcher and since January, 2006 she has been a research assistant at the same department of Kocaeli University. Her research interests include image processing and remote sensing.

Anıl Çelebi (S'00) was born in Ordu, Turkey. He received the B.S. and M.S. degrees in electronics and communication engineering from Kocaeli University, Kocaeli, in 2002 and 2005 respectively. He is currently working toward the Ph.D. degree at the Graduate School of Natural and Applied Sciences, Kocaeli University.

His major research interests include very large scale integration (VLSI) design and implementation for analog/mixed signal systems, image processing systems, and video coding systems.

Sarp Ertürk (M'99**)** received his B.Sc. in Electrical and Electronics Engineering from Middle East Technical University, Ankara in 1995. He received his M.Sc. in Telecommunication and Information Systems and Ph.D. in Electronic Systems Engineering in 1996 and 1999 respectively from the University of Essex, U.K. From 1999 to 2001 he carried out his compulsory service at the Army Academy, Ankara. He is currently appointed as Full Professor at Kocaeli University, where he worked as Assistant Professor between 2001 and 2002, and Associate Professor between 2002 and 2007. His research interests are in the area of digital signal and image processing, video coding, remote sensing and digital communications.

TABLE I
BAND INDEX NUMBERS OBTAINED AT THE FIRST BAND SELECTION (FBS) STEP AND THE SECOND BAND SELECTION (SBS) STEP.

Data Set	FBS	SBS
INDIAN PINE	5, 6, 7, 31, 33, 34, 75, 76, 100, 101, 102, 111, 112, 113, 114, 145, 146 , 147, 148, 166, 167, 168 , 169, 173, 216	5, 75, 169
CUPRITE	104, 105, 106, 116, 117 150, 151, 152, 170, 171 172, 176, 177, 213, 216	116, 152, 216

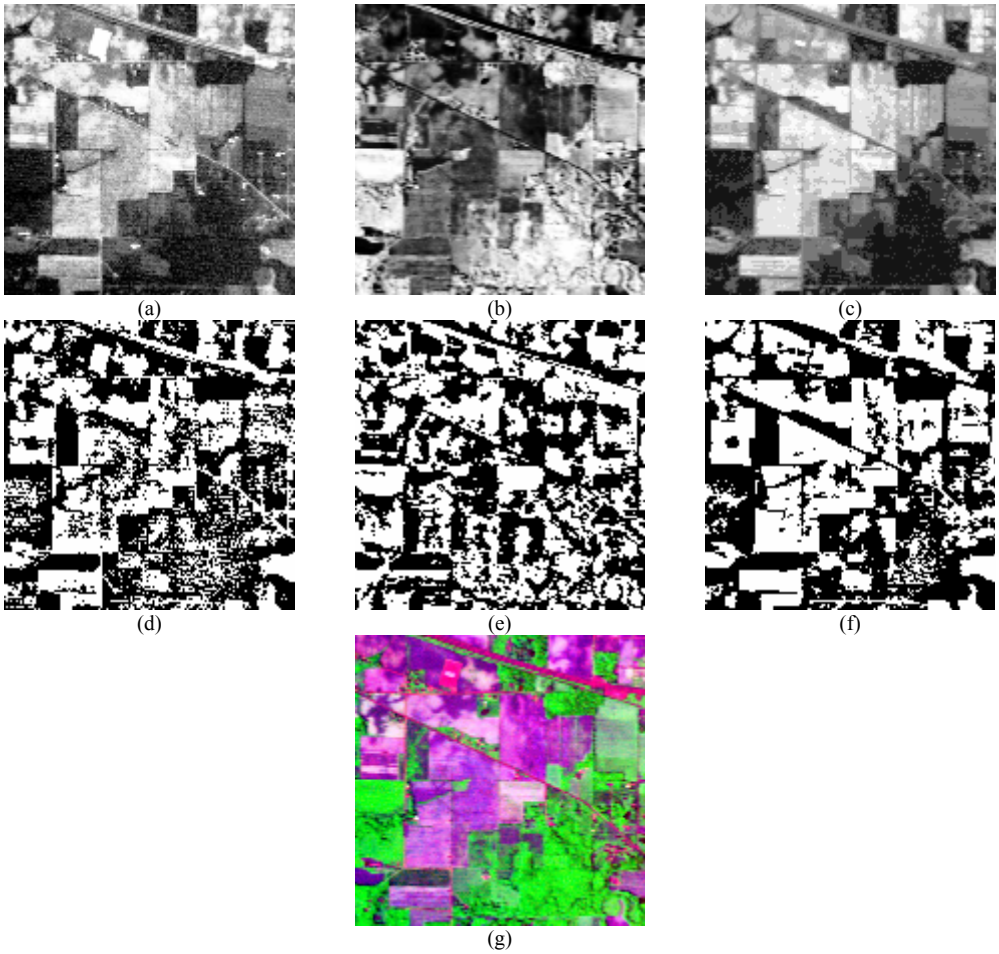

Fig.8. (a) Band # 5 , (b) band # 75 , (c) band # 169 (d) 1BT band # 5 (transition number is 9724), (e) 1BT band # 75 (transition number is 8236) (f)1BT band # 169 (transition number is 6262) (g) RGB color display of these bands for the Indian Pine data set.

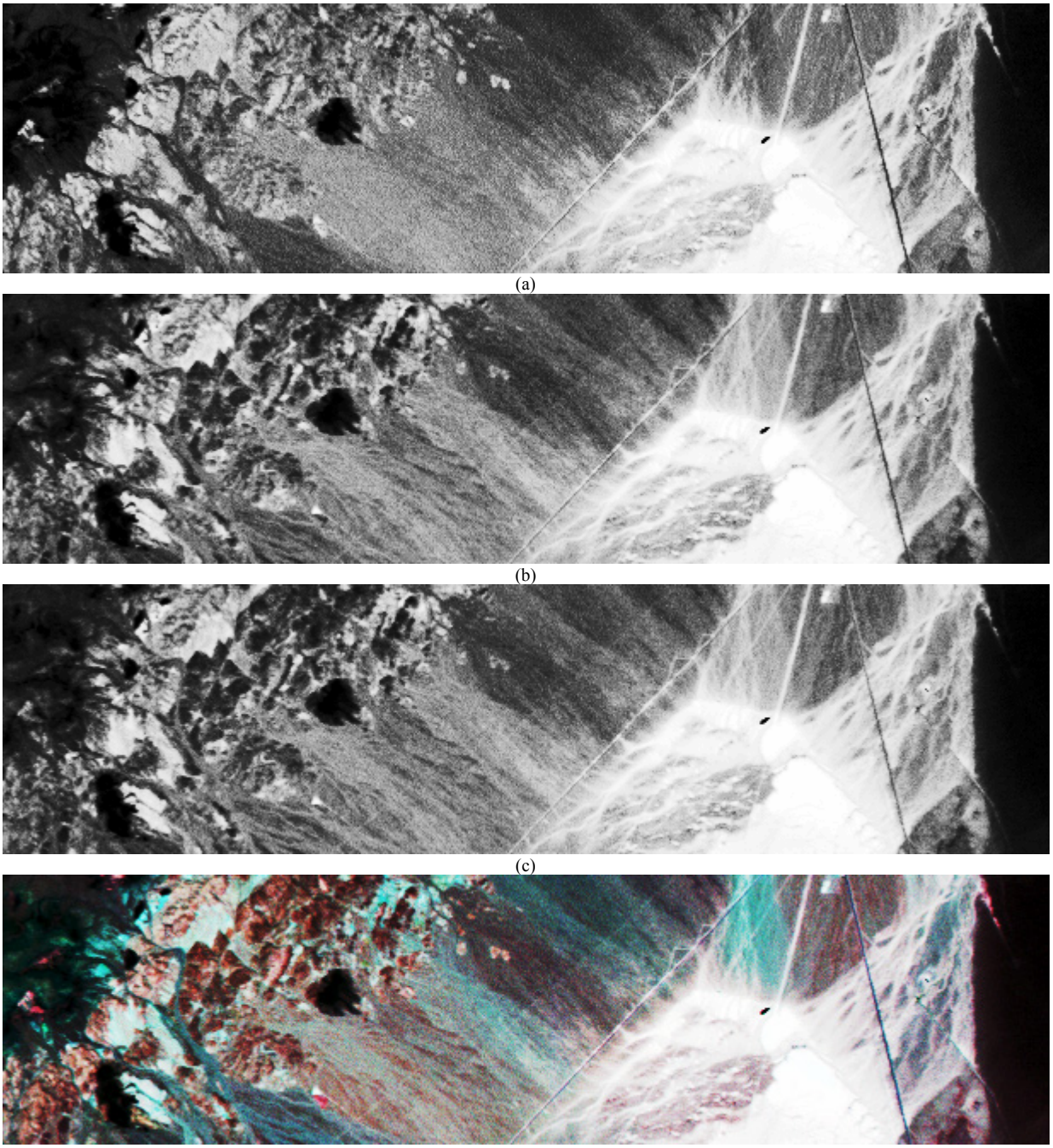

(a)

(b)

(c)

(d)

Fig.9. (a) Band # 216 (transition number is 55218), (b) band # 152 (transition number is 45703) (c) band # 116 (transition number is 45606) (d) RGB color display of these bands for the Cuprite data set.

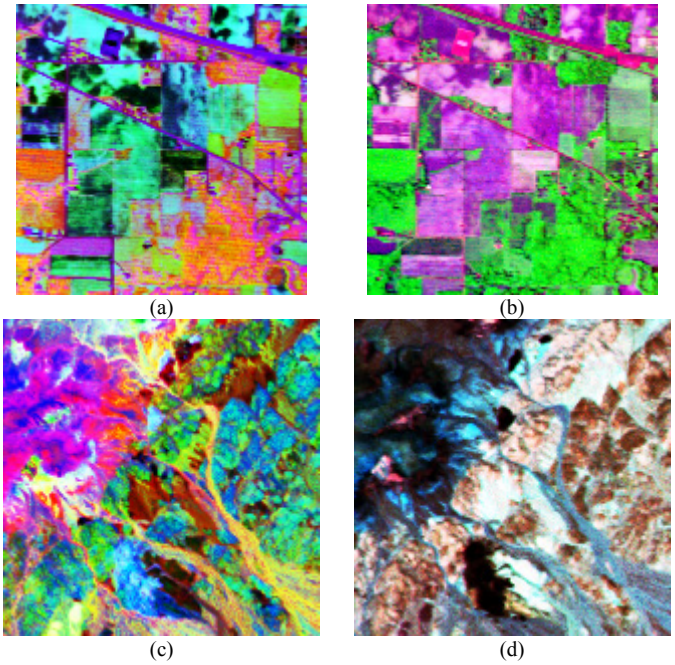

(a) (b) (c) (d)

Fig.10. (a) PCA color display results for the Indian Pine data (b) proposed color display results for the Indian Pine data (c) PCA color display results for part of the Cuprite data, (d) proposed color display results for part of the Cuprite data.

TABLE II

CORRELATION COEFFICIENTS BETWEEN THE RGB COMPONENTS OF THE INDIAN PINE IMAGE OBTAINED BY THE PROPOSED APPROACH.

Proposed Algorithm	R	G	B
R	1	-0.4877	0.9070
G	-0.4877	1	0.5193
B	0.9070	0.5193	1

TABLE III

CORRELATION COEFFICIENTS BETWEEN THE RGB COMPONENTS OF THE INDIAN PINE IMAGE OBTAINED BY THE PCA BASED APPROACH.

PCA	R	G	B
R	1	0.0820	0.0740
G	0.0820	1	8.2694e-004
B	0.0740	8.2694e-004	1

TABLE IV

CORRELATION COEFFICIENTS BETWEEN THE RGB COMPONENTS OF THE CUPRITE SUB-IMAGE OBTAINED BY THE PROPOSED APPROACH

Proposed Algorithm	R	G	B
R	1	0.8360	0.8211
G	0.8360	1	0.9809
B	0.8211	0.9809	1

TABLE V

CORRELATION COEFFICIENTS BETWEEN THE RGB COMPONENTS OF THE CUPRITE SUB-IMAGE OBTAINED BY THE PCA BASED APPROACH

PCA	R	G	B
R	1	0.0127	0.0230
G	0.0127	1	0.0127
B	0.0230	0.0127	1

TABLE VI

CORRELATION COEFFICIENTS BETWEEN THE RGB COMPONENTS OF THE ENTIRE CUPRITE IMAGE OBTAINED BY THE PROPOSED APPROACH.

Proposed Algorithm	R	G	B
R	1	0.8933	0.8853
G	0.8933	1	0.9811
B	0.8853	0.9811	1